



This is a repository copy of *Superior magnetodielectric properties of CoZnNd ferrites/GNPs composite materials for potential applications.*

White Rose Research Online URL for this paper:

<https://eprints.whiterose.ac.uk/202477/>

Version: Accepted Version

Article:

Arshad, M.I. orcid.org/0000-0002-8251-4229, Mehmood, K., Amin, N. et al. (2 more authors) (2023) Superior magnetodielectric properties of CoZnNd ferrites/GNPs composite materials for potential applications. *Composites Communications*, 39. 101571. ISSN 2452-2139

<https://doi.org/10.1016/j.coco.2023.101571>

Article available under the terms of the CC-BY-NC-ND licence (<https://creativecommons.org/licenses/by-nc-nd/4.0/>).

Reuse

This article is distributed under the terms of the Creative Commons Attribution-NonCommercial-NoDerivs (CC BY-NC-ND) licence. This licence only allows you to download this work and share it with others as long as you credit the authors, but you can't change the article in any way or use it commercially. More information and the full terms of the licence here: <https://creativecommons.org/licenses/>

Takedown

If you consider content in White Rose Research Online to be in breach of UK law, please notify us by emailing eprints@whiterose.ac.uk including the URL of the record and the reason for the withdrawal request.



eprints@whiterose.ac.uk
<https://eprints.whiterose.ac.uk/>

Superior Magnetodielectric Properties of CoZnNd ferrites/GNPs Composite Materials for Potential Applications

Muhammad Imran Arshad^{a,c}, Kiran Mehmood^{a*}, Nasir Amin^a, N. A. Morley^b, Nguyen Thi Kim Thanh^{c,d}

^a*Department of Physics, Government College University, Faisalabad, 38000, Pakistan.*

^b*Department of Materials Science and Engineering, The University of Sheffield, UK, S1 3JD.*

^c*Biophysics Group, Department of Physics and Astronomy, University College London, Gower Street, London, WC1E 6BT, UK*

^d*UCL Healthcare Biomagnetics and Nanomaterials Laboratories, 21 Albemarle Street, London, W1S 4BS, UK.*

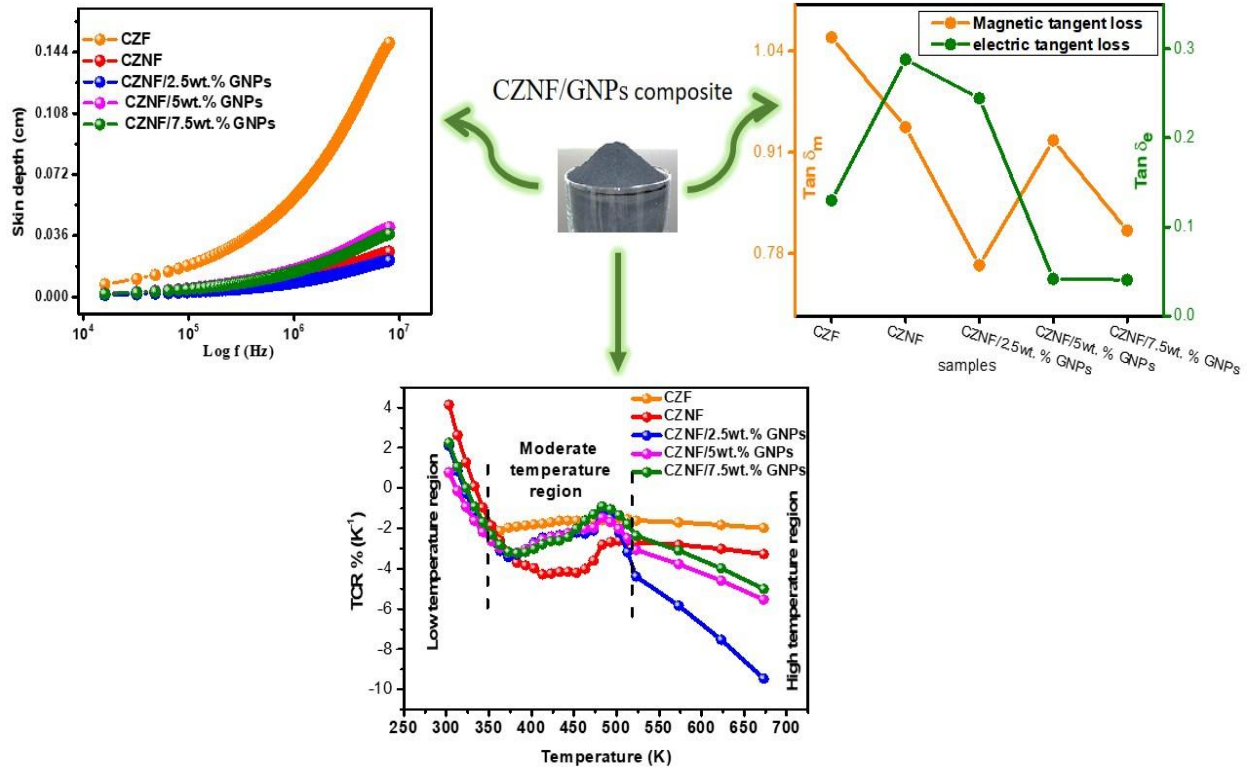
*Corresponding Author: kiranjaspal@yahoo.com

Abstract

This research explores the effect of graphene nanoplatelets (GNPs) on structural, electrical, magnetic and dielectric properties along with surface morphology of CoZnNd ferrites (CZNF), synthesized through sol-gel auto combustion route. The results exhibited that CZNF particles were dispersed on GNPs, which modified the structural and electromagnetic characteristics of CZNF. Moreover, SEM micrographs revealed the reduction in agglomeration with inclusion of GNPs. Additionally, resistivity was increased in the ferro region and decreased in the para region with rising temperature. TCR for CZNF/2.5wt. %GNPs composite was recorded as -3.49 % at 371 K. Excellent magnetodielectric properties were observed for CZNF/2.5wt. %GNPs composite, i.e. $M_s = 141.76$ emu/g and $H_c = 81.2$ Oe along with minimum $\tan \delta_m$ and skin depth. On the basis of studied parameters, CZNF/2.5wt. %GNPs composite is appropriate for high frequency micro wave shielding applications, inductors, filters, bolometers and switching devices.

Keywords: Nanocomposites; graphene nanoplatelets; ferrites; dielectric; switching field distribution (SFD).

Graphical Abstract



Highlights

- Ferrite/GNPs nanocomposites were fabricated *via* sol-gel auto combustion strategy.
- The peak position ($-3.49 \% K^{-1}$) of temperature *versus* TCR percentage plots occurs at 371 K for CZNF/2.5wt%GNPs nanocomposite.
- The magnetic tangent losses and skin depth was minimum for CZNF/2.5wt%GNPs nanocomposite.
- Variation in magnetic parameters confirmed the role of GNPs.
- Soft magnetic nature was linearly increased with GNPs substitution because, Coercivity was decreased.

1 Introduction

Graphene an allotrope of carbon is known as strongest material in the world. [1]. Graphene is a two dimensional (2-D) arrangement of atoms with thickness of only one atom, which holds unique mechanical, chemical and physical properties [2]. Structure of graphene comprises with six carbon atoms arranged in a regular hexagonal fashion with a single atom thickness, large aspect ratio and superior flexibility. This network of six-atom rings composed of one carbon (C) atom bonded to three other carbon (C) atoms with a C-C bond length of 1.42 Å and bond angle of 120°. Moreover, due to tiniest thickness graphene (derivative of carbon) could not exist in free form. Graphene based studies have been a rapid growth due to their synthesis, unique properties and potential candidate for many applications [3,4]. Additionally, the production cost of multilayer graphene on large scale is very low as compared to other allotropes of carbon. Owing to these properties many graphene based ferrites composites have been studied extensively [1]. Ferrites/graphene composites are very famous for water treatment, diagnostic analysis, photocatalytic phenomena, electronic devices and drug transportation [5,6].

Nanocomposites are polyphase solid materials fabricated by the amalgamation of different materials whose characteristics are substantially changed at nano-scale as compared to their parent elements. Surface to volume ratio of nanocomposites is high [7]. Owing to different materials as a single element the properties of nanocomposites are highly improved. Nanocomposites of graphene and rare-earth doped ferrites are remarkable materials attributable to their nontoxic nature and exceptional magnetic, chemical, optical and electrical properties. Research work on the synthesis of graphene based rare-earth doped ferrite nanoparticles is very vast [8–10]. Properties of composites can be tuned by changing composition of precursors and selection of doped rare earth element. Accumulation problem of ferrites can be resolved by the addition of graphene [6]. Though, defects and disorders are appeared in the crystal structure due to the presence of different electronic structures, distribution of cations and valance states, which are responsible for unique dielectric and magnetic properties in composites [5,11].

Magnetodielectric (MD) materials are an important class of materials that exhibit dielectric and magnetic properties in a single phase. Magnetodielectric materials have been widely investigated due to their potential applications including magnetic sensors, high frequency microwave absorbers, antenna miniaturization, data storage devices, catalysis, etc.[11–14].

Generally, magnetodielectric materials are formed by combining material with high electric permittivity along with material having high magnetic permeability. In this research work, we considered Cobalt Zinc ferrites (CZF) and graphene nanoplatelets (GNPs). The CZF are magnetic materials hence exhibit considerable magnetic permeability while GNPs are material with high electric permittivity. The CZ ferrites are regarded as soft magnetic materials with extraordinary electrical and magnetic properties [15]. On the other hand, insertion of GNPs stimulates formation of space charges which promote the interfacial polarization. Due to this phenomenon dielectricity of material increases [16].

Herein, we report on sol-gel auto combustion synthesis of $\text{Co}_{0.5}\text{Zn}_{0.5}\text{Fe}_2\text{O}_4$ (CZF), $\text{Co}_{0.5}\text{Zn}_{0.5}\text{Nd}_{0.03}\text{Fe}_{1.97}\text{O}_4$ (CZNF) and its composites with GNPs. The effect of different stoichiometric proportions of graphene nanoplatelets (GNPs) was studied on structural, electrical, morphological, dielectric and magnetic properties of ferrites/GNPs composites. In this research work five samples were synthesized i.e. CZF, CZNF, CZNF/2.5wt.%GNPs, CZNF/5wt.%GNPs and CZNF/7.5wt.%GNPs.

2 Experimental procedure

Co nitrate hexahydrate [$\text{Co}(\text{NO}_3)_2 \cdot 6\text{H}_2\text{O}$], Zinc acetate [$\text{Zn}(\text{CH}_3\text{COO})_2 \cdot 2\text{H}_2\text{O}$], Iron nitrate nonahydrate [$\text{Fe}(\text{NO}_3)_3 \cdot 9\text{H}_2\text{O}$], Neodymium nitrate hexahydrate [$\text{Nd}(\text{NO}_3)_3 \cdot 6\text{H}_2\text{O}$] and graphene nanoplatelets (GNPs) were used as precursors. GNPs with particle size 25 μm and surface area 120-150 m^2/g were used to form composites. Citric acid [$\text{C}_6\text{H}_8\text{O}_7$] was picked out as a combustible agent. Citric acid and other metal solutions were mixed at 1:1.2 with stoichiometric calculations. Liquid Ammonia was added drop wise to obtain a pH of 7 while keeping the resulting solution at magnetic stirrer. Heating with continuous stirring led to the formation of sticky gel, which was in dark fluffy powder by auto combustion process. The resultant powder of as-prepared samples was obtained by grinding and calcination at 850°C for 5 hours. Complete synthesis process is presented in Fig. 1.

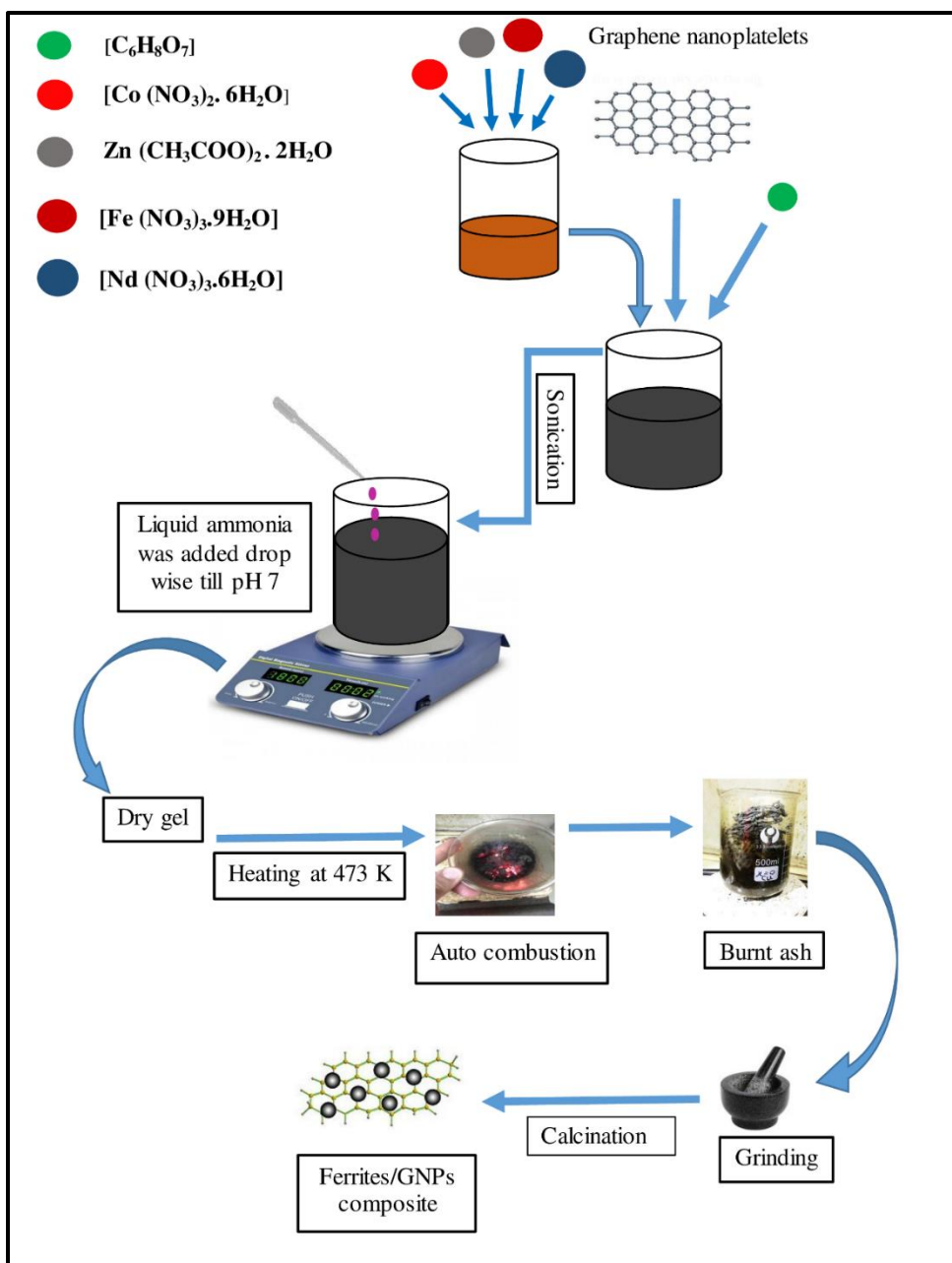


Fig. 1: Schematic synthesis process of CZNF/GNPs composite

3 Results and discussion

Structure of as-prepared samples was evaluated by XRD and Raman analysis. Fig. 2(a) represents the XRD pattern whose peaks were indexed to miler indices (220), (311), (222), (400), (422) and (511, appearance of major peak in XRD spectra indexed at (311) indicated spinel structure of all samples. A slight peak shift was detected in the (311) plane attributed to the substitution of Nd³⁺ and GNPs (Fig. 2(b)). However, the CZNF/GNPs composites revealed that

GNPs peaks indexed to (0 0 2) and (0 0 4) were slightly shifted towards lower 2θ due to deformation in structure of GNPs by spinel structure of ferrite and presence of rare-earth [17].

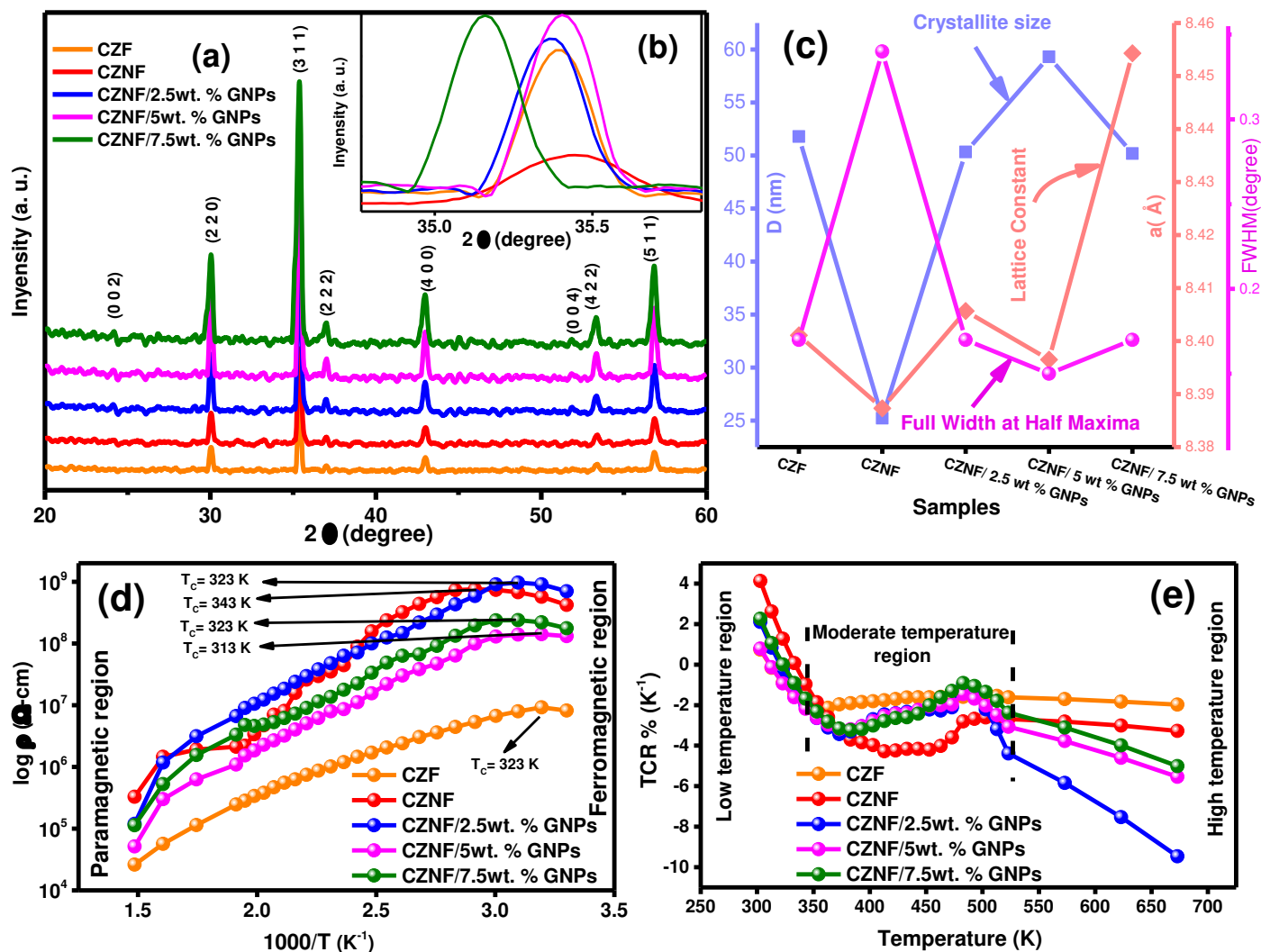


Fig. 2: (a) XRD patterns (b) peak shift (c) D, a and FWHM versus samples (d) Arrhenius plot (e) TCR%

Grain size calculated from XRD was found in the range of 25.2nm to 59.3nm. Reduction in grain size by Nd^{3+} doping in CZF matrix may attributed to small solubility of Nd^{3+} , hence more Nd^{3+} are located at grain boundaries and pressure of doping Nd^{3+} at grain boundaries indicated decreased lattice constant (a) grain growth of CZNF. More energy is required for the formation and growth of CZNF as compared to CZF [18]. Enhancement in grain size was seen with the inclusion of GNPs in CZNF [10] but not in a regular manner. Variation in crystallite size, lattice constant and FWHM regarding samples is presented in Fig. 2 (c)

Raman analysis was performed to further reveal structure of as-prepared samples and corresponding Raman spectra is presented in Fig. 3. Raman spectra exhibits the three major active modes of spinel ferrites including E_g , T_{2g} , and $A_{1g}(2)$ are detected around 331, 470 and 640 cm^{-1} [19]. However, three bands around 1304 cm^{-1} (D-band) and 1670 cm^{-1} (G-band). Which indicates ferrite particles are successfully dispersed on GNPs. The D and G bands are attributed to defect and disorderliness of GNPs [20].

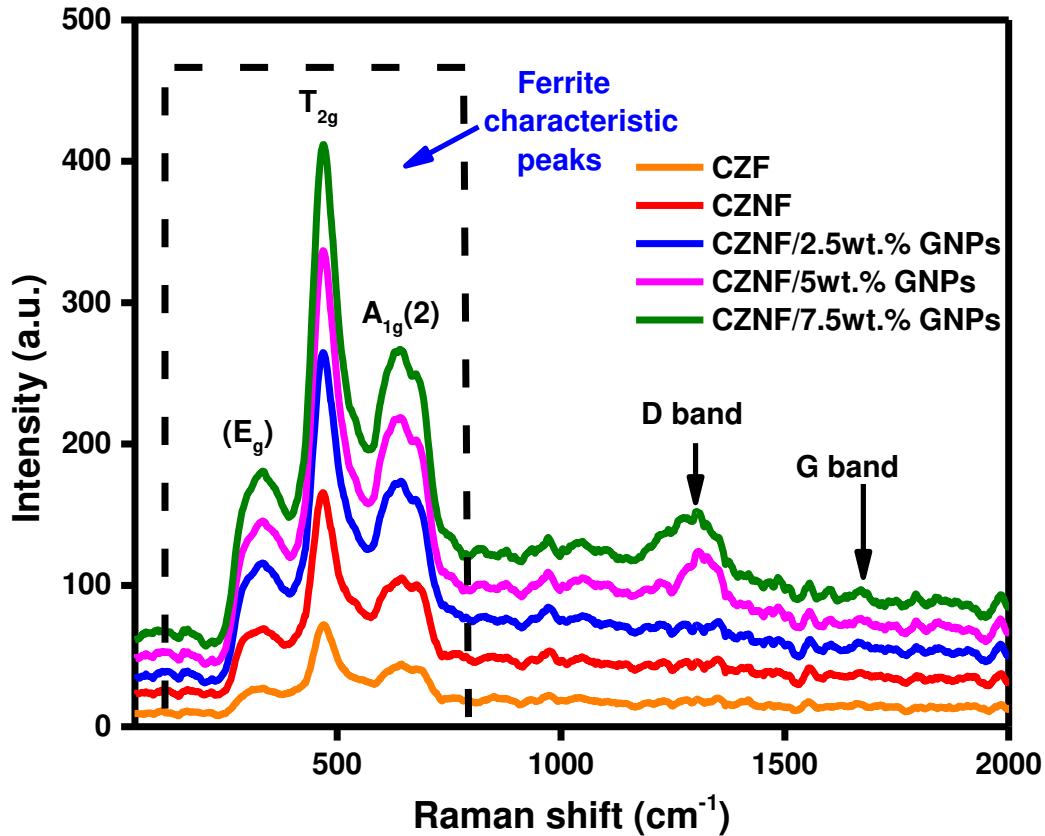


Fig. 3: Raman spectra of CZF, CZNF and CZNF/GNPs composites

Electrical properties of ferrites and its composites can be well explained by measuring temperature-dependent resistivity. Fig. 2(d) illustrates $\log \rho$ versus $10^3/T$ (Arrhenius plots) of all samples. Curie temperature (T_c), a transition temperature divides the log of resistivity curves into two separate region such as ferro region and para region. Reduction in resistivity with rising temperature (T) demonstrates the semiconducting nature of as-prepared samples because the drift mobility of charge carriers increases with a hike in T . Ferrites conduct by electron hopping amongst same ions such as Fe^{3+} and Fe^{2+} ions with different oxidation number which are distributed arbitrarily between lattice sites stated by Verwey's hopping mechanism [21].

Temperature coefficient of resistance ($TCR\% = [1/\rho][d\rho/dT] \times 100$ Here, $T =$ temperature, $\rho =$ resistivity) is an important parameter for estimating device applications in bolometers and optoelectrical devices [22]. The peak position of $TCR\%$ values from Fig. 2(e) were $-2.10K^{-1}$, $-4.28K^{-1}$, $-3.49K^{-1}$, $-3.22K^{-1}$, $-3.22K^{-1}$ at 363K, 414K, 371K, 382K and 382K respectively. Factors that could affect peak values of $TCR\%$ are sintering temperature and time [23].

Morphology of all samples was identified by SEM and AFM. Fig. 4 (A) illustrates that ferrite particles are not uniform in size and tend to aggregate up to some extent because of their strong magnetic interactions and high surface energy [24]. Fig. 4A (a-e) demonstrates that with increasing content of GNPs agglomeration of ferrite particles was reduced. AFM images shown in Fig. 4B exhibits roughness of surfaces with GNPs inclusion, indicating that ferrite particles are fused on GNPs surface. Synthesis route and dispersion of ferrite particles on GNPs sheets play a key in modifications of composites [25].

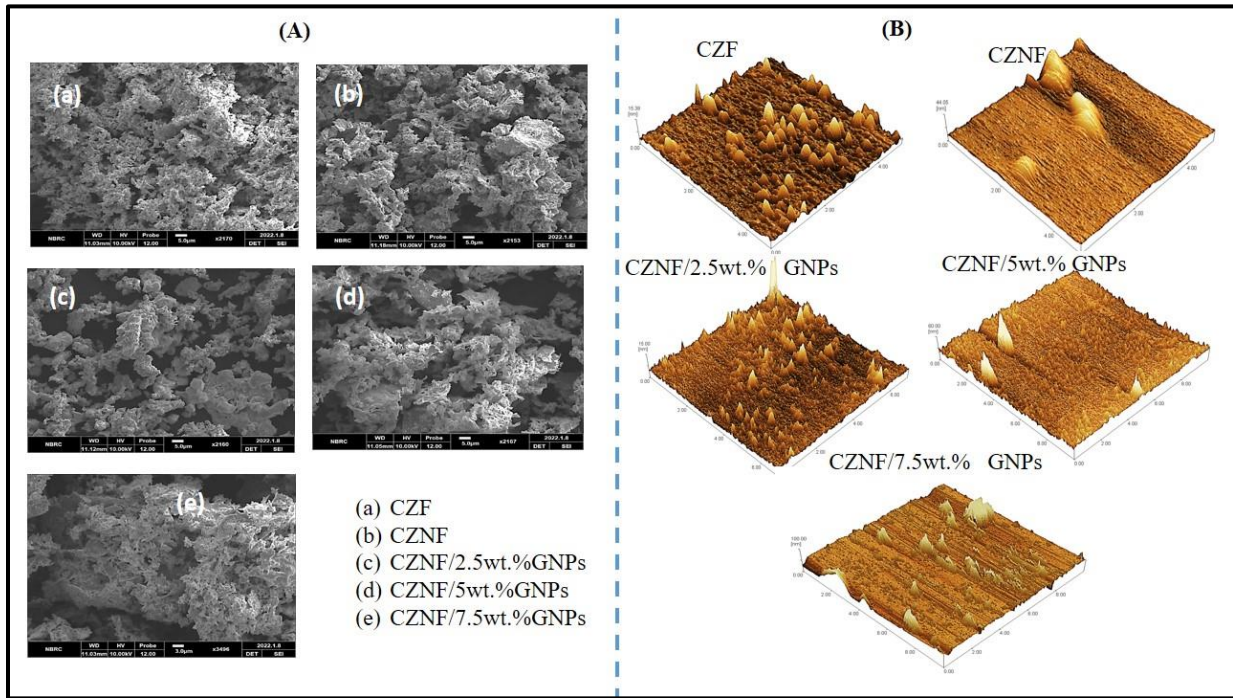


Fig. 4: (A) SEM micrographs (a-e) (B) 3D AFM images of all samples

Dielectric behavior, one of the significant properties of ferrite/GNPs composites was studied at room temperature between 4Hz to 8MHz. Different parameters like chemical composition of materials, crystallite size, synthesis method, sintering temperature and distribution of metal ions

in the unit cell are responsible for dielectric behavior [5]. In ferrites charge carriers are transported through hopping among the atoms of octahedral sites but with different oxidation states i.e. Fe^{2+} and Fe^{3+} states. However, in ferrite/GNPs composites the loss mechanism is related to the transportation of charge carriers through hopping and migration over interlocked GNPs grid. The dielectric polarization in ferrites is associated with conduction mechanism [26]. Though, in ferrite/GNPs composites many defects which are created on GNPs during synthesis process stimulate dipole polarization [27]. With rising frequency variation in dielectric loss is due to the orientation of induced dipoles with external frequency [28]. Interfacial polarization which is the result of formation of heterogeneous interfaces including ferrite/ferrite and ferrite/GNPs. These manifold polarizations are responsible for dielectric loss [29]. Simultaneously, ferrite (magnetic) particles introduce magnetic loss which comprises magnetic resonance and induction of eddy current [30]. These all phenomenon are showed in Figs. 5(a-e).

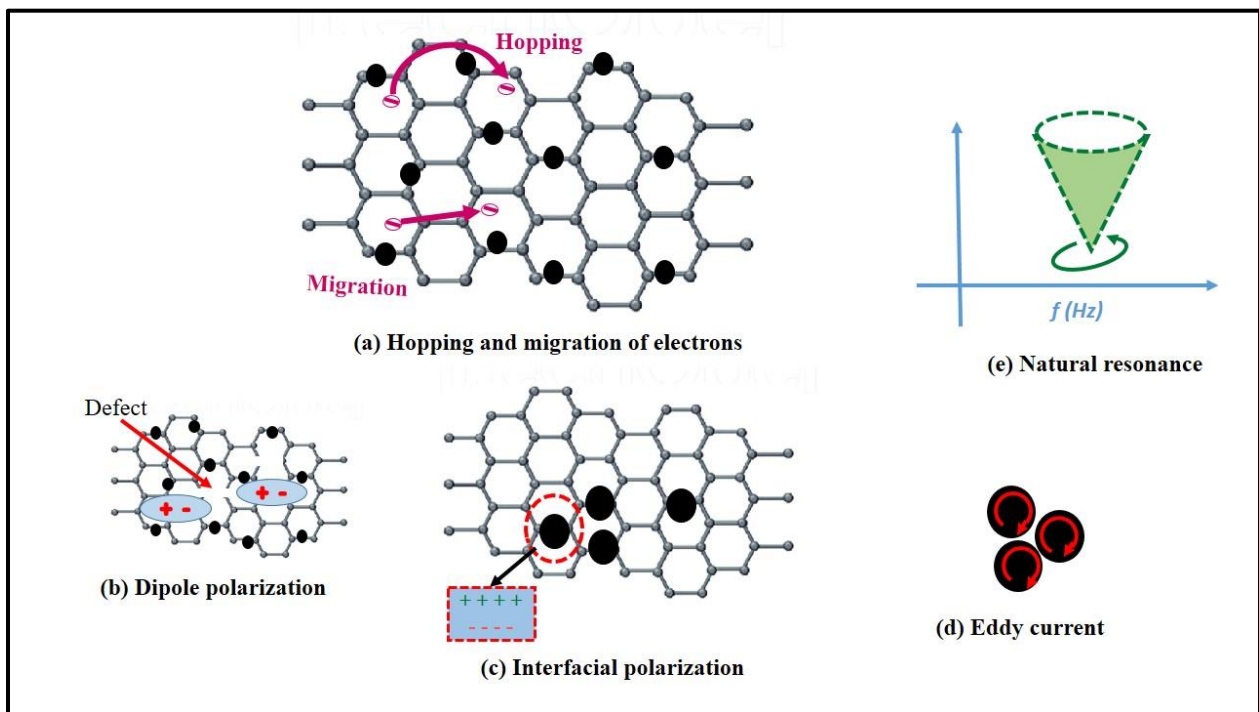


Fig. 5: Mechanisms possibly affect dielectric properties

Real part of permittivity (ϵ') and imaginary part of permittivity (ϵ'') are plotted in Figs. 6 (a,b) respectively. Both ϵ' and ϵ'' exhibited continuously decline curve with increasing frequency hence, follows the Debye's conduction theory at large values of frequency [30,31]. At low frequency ϵ'

increased up to 48 with Nd^{3+} doping and then suddenly decreased to 23 with GNP 2.5wt.%, which was decreased up to 20.6 for 7.5wt.%GNPs, indicating decreasing capability of polarization with GNP content [30]. At high frequency ϵ' was irregularly decreased with Nd^{3+} and GNP. ϵ'' was increased up to 13.9 with Nd^{3+} doping [32] which was regularly decreased up to 0.80 with GNP addition at low frequency. $\text{Tan } \delta_e$, referred as tangent loss ($\text{Tan } \delta_e = \epsilon''/\epsilon'$) is presented in Fig. 6(c). Loss capability of dielectric materials for electromagnetic energy is represented by ϵ'' . Therefore, the variation in tangent loss plot indicated low dielectric loss with inclusion of GNP in CZNF. The dielectric relaxation, domain wall dielectric resonance and electrical conduction are key phenomena to dissipate energy [21,33].

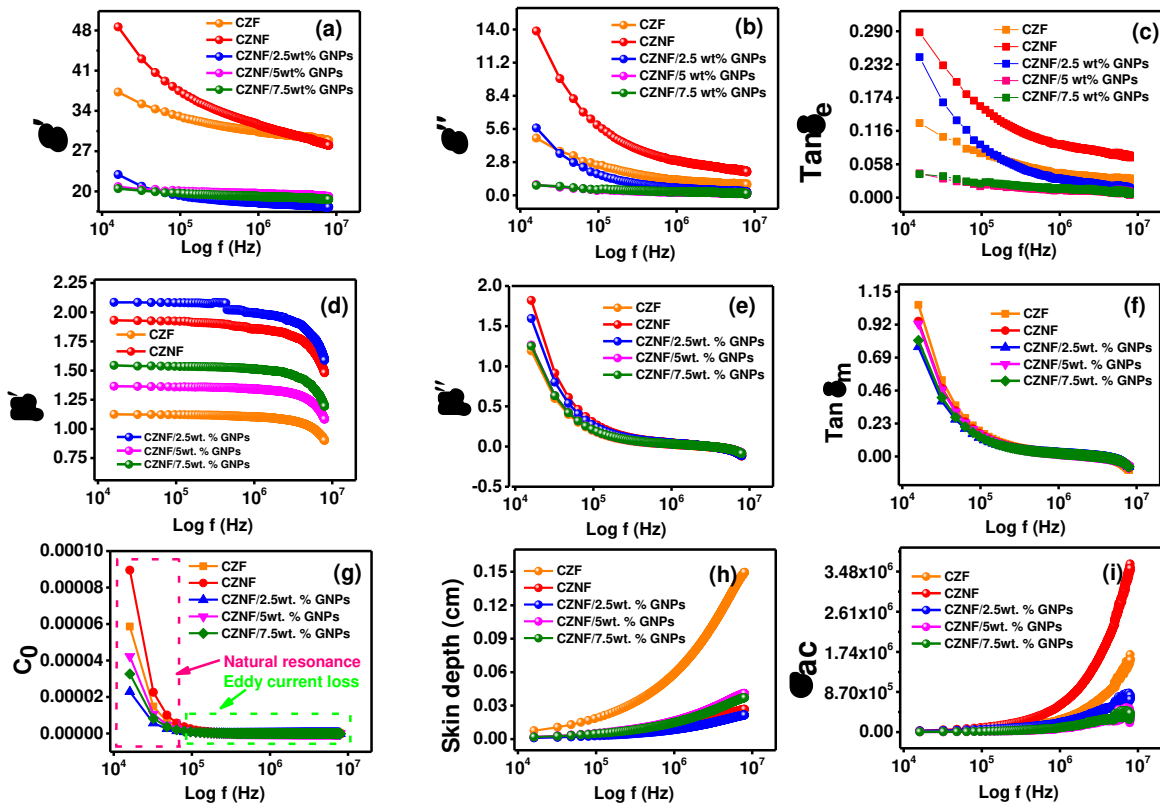


Fig. 6: Frequency versus (a) ϵ' (b) ϵ'' (c) $\text{Tan } \delta_e$ (d) μ' (e) μ'' (f) $\text{tan } \delta_m$ (g) C_0 (h) skin depth (i) σ_{ac}

Fig. 6 (d,e) depicts frequency dependent real (μ') and imaginary ($\mu'' = \mu' \times \text{tan} \delta_m$) parts of complex permeability, indicates the storage ability and dissipation capacity of magnetic energy respectively [34]. Real part of complex permeability was independent of low frequency and

suddenly reduced at high frequency. At low frequency μ'' was observed dependent on frequency and became independent at higher frequency as displayed in Fig. 6(e). Moreover, μ' was significantly improved by Nd^{3+} and GNPs addition. Whereas, μ'' was decreased substantially with increasing GNPs substitution in CZNF sample. Magnetic tangent loss or magnetic loss factor ($\tan \delta_m$) referred to the energy loss due to the phase delay among induced magnetic field and applied magnetic field inside a magnetic material, displayed in Fig. 6(f). Magnetic tangent loss ($\tan \delta_m$) was dominated by CZF, which was reduced by Nd^{3+} and GNPs substitution but not in a regular manner. Hysteresis loss, residual loss and eddy current loss are the general forms of magnetic tangent loss inside a magnetic material [32,35]. Eddy current loss is caused by the generation of eddy current by induction mechanism inside a magnetic material placed in an alternating magnetic field. The residual loss is generally comprises of natural resonance, exchange resonance and domain wall resonance during magnetization of a magnetic material [35]. Magnetic loss can be evaluated by C_0 ($C_0 = \mu''(\mu')^{-2}f^{-1}$) versus frequency plot [29,35,36], Fig. 6(g).

Fig. 6(h) demonstrates the variation in skin depth ($s = [1/2\pi][\sqrt{\mu f/\rho}]$) against frequency [37]. Skin depth slightly increases with increasing frequency. Minimum skin depth of 0.21mm at 8MHz was observed for CZNF/2.5wt.% GNPs composite. The *ac* conductivity (σ_{ac}) was reduced with the inclusion of GNPs as compared to pure CZF and CZNF samples Figs. 6(i).

Fig. 7(a,b) exhibited the inverse relation of real (Z') and imaginary (Z'') parts of impedance with frequency. As Z' and Z'' remain unaltered after 10^6 Hz showing that conduction mechanism is prevailing at high frequency because of electron hopping [38]. Q factor is an important dielectric parameter to predict the efficiency of electrical components and devices by establishing relation between stored energy and dissipated energy shown in Fig. 7(c). Q factor of ferrite/GNPs composites is greater than pure CZF and CZNF samples.

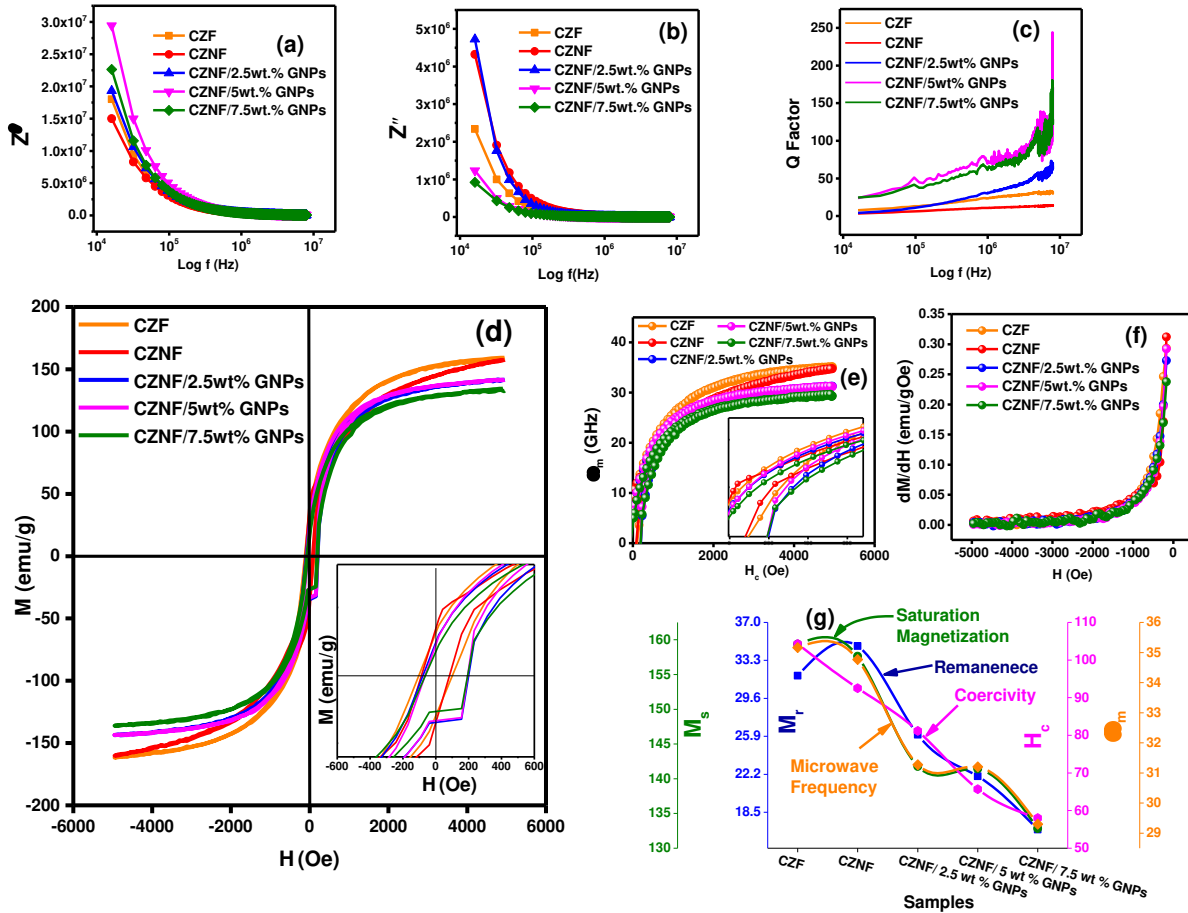


Fig. 7: Frequency *versus* (a) Z' (b) Z'' (c) Q factor, (d) M-H Loops, H *versus* (e) ω_m and (f) dM/dH , (g) samples *versus* M_s , H_c , M_r , ω_m

The Hysteresis loops (M-H loop) of ferrites and its composites are shown in Fig. 7(d), exhibiting soft ferromagnetic nature. Properties of hysteresis loops are highly affected by microstructures, synthesis methodology, sintering temperature, purity and distribution of cations among A and B sites [17,36,39]. Variation in magnetic parameters including saturation magnetization, remanence, coercivity and microwave frequency *versus* samples is illustrated in Fig. 7(g). It was observed that saturation magnetization and other magnetic parameters were reduced with Nd^{3+} doping. Saturation magnetization attributed to different magnetic moments at A and B sites in ferrites. Hence, the overall saturation magnetization in ferrites is the result of difference in magnetization at both sites. Generally, in rare earth doped ferrites Fe^{3+} are replaced by RE^{3+} ions which may reduce magnetization due to the small magnetic moments of RE^{3+} ions

as compared to Fe^{3+} ions. Moreover, when nonmagnetic GNPs are added to CoZn ferrites, the magnetic moments tend to further decrease in saturation magnetization [40,41].

The figures illustrate that the hysteresis curves are not wide, with a relatively small coercive magnetic field classifying the studied samples as soft magnetic materials. The small coercive force values permit easy magnetization and demagnetization with limited losses. This observation suggests that all samples may be suitable for magnetic applications conditioned by low energy losses

Saturation magnetization and remanence of synthesized samples were found between 159.37 – 132.83 emu/g and 34.7 – 1.81 emu/g respectively. The figures illustrate narrow M-H loops, which are attributed to small values of coercivity. These low values of coercivity classify the synthesized material as soft magnetic materials. Therefore, magnetization and demagnetization of material offer limited losses which suggests the suitability of material for low loss energy devices. Additionally, H_c was reduced from 104.3 – 92.5 Oe with Nd doping which was further reduced in ferrite/GNPs composites up to 58.04 Oe due to reduced spin order of GNPs. The low coercivity of as-prepared samples make them potential candidate for microwave absorption applications [42]. According to literature review Riaz *et al.*, reported saturation magnetization of Nd doped CoZn ferrites from 81.5–66.2 emu/g, Coercivity from 241.24–162.13 Oe and remanence from 10.84 - 9.22 emu/g [43]. Kokare *et al.*, prepared Nd doped NiCo ferrites *via* sol-gel auto combustion method and claimed saturation magnetization between 51.85 – 19.70 emu/g, remanence from 31.75 emu/g to 13.83 emu/g and coercivity from 1396.02 Oe to 813.73 Oe [41]. Almessiere *et al.*, reported saturation magnetization, coercivity and remanence of CoNdCe ferrites with $x=0.03$ and calculated values were 58.51 emu/g, 1131.5 Oe and 21.12 emu/g respectively [44]. The microwave frequency $\omega_m = 8\gamma\pi^2 M_s$, Here, γ = gyromagnetic fraction = 2.8 MHz/Oe [21] is presented in Fig. 7(e). The microwave frequency (35.16 – 29.30 GHz) was found to decrease with addition of Nd^{3+} ions and GNPs correspondingly

In Fig. 7(f) switching field distribution (SFD) curves are analyzed by using dM/dH (first derivative of demagnetization data) *versus* applied field H . SFD curves reveal the exchange coupling interactions (A-B interactions) among metal cations at their lattice sites. Magnetic characteristics in spinel ferrites are consequence of exchange coupling interactions among Fe-ions and spin coupling of 3d electrons [24,45]. Additionally, magnetization of ferrites be influenced by the distribution of Fe^{3+} ions between octahedral and tetrahedral sites along with spins on the

surface of nanoparticles [46]. Smooth lines at high reverse fields indicates strong magnetic interactions of cations. The rapid increasing behavior of dM/dH data at low fields indicates the SFD behavior of under investigation samples [45]. Though, the CZNF samples possesses highest SFD value and CZNF/7.5wt.% GNPs nanocomposite possess smallest value. The doping of Nd^{3+} (0.983 Å) ions with Fe^{3+} (0.64 Å) ions, results in a lattice distortion, which improved the magnetic properties of the material. Instead non-magnetic nature and low crystallinity of GNPs are responsible for the variation in magnetic properties of ferrite/GNPs nanocomposites. However, it can be observed from magnetic data that all magnetic parameters systematically increased and decreased with the addition of Nd and GNPs. The small particle size along with high values of magnetization and low Coercivity can bring innovative changes in the miniaturization of devices for high- frequency operating devices [24].

Conclusion

This research work demonstrates the sol-gel auto combustion synthesis route for CZNF/GNPs composites. The combination of XRD and Raman analysis revealed the existence of spinel phase in all samples. SEM micrographs showed a decrease in agglomeration with the substitution of GNPs in CZNF/GNPs composites. AFM results were supported by SEM results and revealed the dispersion of ferrite particles on GNPs and roughness of surface. Crystallite size was measured through XRD analysis and was found between 25.2 nm and 59.3nm. Resistivity at 303 K was found 1.30×10^8 (Ω -cm) for CZNF/5wt. % GNPs nanocomposite sample. TCR peak value for CZNF/2.5wt%GNPs was observed as $-3.49 \% K^{-1}$ at 371 K. Dielectric study reveals that $Tan\delta_m$ and magnetic loss of CZNF/2.5wt%GNPs composite was minimum with minimum skin depth of 0.21 mm. The maximum permeability was recorded as 2.07 for CZNF/2.5wt%GNPs composite. Values of M_s and H_c were decreased from 157.63emu/g to 132.82emu/g and 92.5Oe to 58.04Oe respectively with substitution of GNPs. SFD curves indicated strong magnetic interactions of cations at their lattice sites. The dimensions of devices were found to be dependent on range of frequency and properties of materials used. Consequently, encapsulation of CZNF material into nonmagnetic materials such as GNPs is a novel approach to design various devices for microwave shielding applications, switching, inductors and filters.

References

- [1] Z. Hu, G. Tong, D. Lin, Q. Nian, J. Shao, Y. Hu, M. Saei, S. Jin, G.J. Cheng, Laser sintered graphene nickel nanocomposites, *J. Mater. Process. Technol.* 231 (2016) 143–150. <https://doi.org/10.1016/j.jmatprotec.2015.12.022>.
- [2] S. Meti, M.R. Rahman, M.I. Ahmad, K.U. Bhat, Chemical free synthesis of graphene oxide in the preparation of reduced graphene oxide-zinc oxide nanocomposite with improved photocatalytic properties, *Appl. Surf. Sci.* 451 (2018) 67–75. <https://doi.org/10.1016/j.apsusc.2018.04.138>.
- [3] C. Deepa, L. Rajeshkumar, M. Ramesh, Preparation, synthesis, properties and characterization of graphene-based 2D nano-materials for biosensors and bioelectronics _ Elsevier Enhanced Reader.pdf, *J. Mater. Res. Technol.* (2022).
- [4] Q. Zhang, Z. Wu, N. Li, Y. Pu, B. Wang, T. Zhang, J. Tao, Advanced review of graphene-based nanomaterials in drug delivery systems : Synthesis , modification , toxicity and application, *Mater. Sci. Eng. C.* 77 (2017) 1363–1375.
- [5] M. Mahmood, M.A. Yousuf, M.M. Baig, M. Imran, M. Suleman, M. Shahid, M.A. Khan, M.F. Warsi, Spinel ferrite magnetic nanostructures at the surface of graphene sheets for visible light photocatalysis applications, *Phys. B Condens. Matter.* 550 (2018) 317–323. <https://doi.org/10.1016/j.physb.2018.08.043>.
- [6] R.R. Kanna, Structural, morphological and optomagnetic properties of GO/Nd/Cu-Mn ferrite ternary nanocomposite, *Ceram. Int.* 45 (2019) 16138–16146. <https://doi.org/10.1016/j.ceramint.2019.05.132>.
- [7] L.A. Kolahalam, I. V. Kasi Viswanath, B.S. Diwakar, B. Govindh, V. Reddy, Y.L.N. Murthy, Review on nanomaterials: Synthesis and applications, *Mater. Today Proc.* 18 (2019) 2182–2190. <https://doi.org/10.1016/j.matpr.2019.07.371>.
- [8] R.R. Kanna, K. Sakthipandi, N. Lenin, E.J.J. Samuel, Neodymium doped on the manganese–copper nanoferrites: analysis of structural, optical, dielectric and magnetic properties, *J. Mater. Sci. Mater. Electron.* 30 (2019) 4473–4486. <https://doi.org/10.1007/s10854-019-00736-z>.
- [9] J. Li, D. Zhou, W.F. Liu, J.Z. Su, M. Sen Fu, Novel and facile reduced graphene oxide anchored Ni-Co-Zn-Nd-ferrites composites for microwave absorption, *Scr. Mater.* 171 (2019) 42–46. <https://doi.org/10.1016/j.scriptamat.2019.06.018>.
- [10] S. Qamar, M.N. Akhtar, W. Aleem, Z. ur Rehman, A.H. Khan, A. Ahmad, K.M. Batoo, M.

- Aamir, Graphene anchored Ce doped spinel ferrites for practical and technological applications, *Ceram. Int.* 46 (2020) 7081–7088. <https://doi.org/10.1016/j.ceramint.2019.11.200>.
- [11] T. Warski, J. Kubacki, D. Łukowiec, R. Babilas, P. Włodarczyk, Ł. Hawełek, M. Polak, B. Jóźwik, M. Kowalczyk, A. Kolano-Burian, A. Radoń, Magnetodielectric and low-frequency microwave absorption properties of entropy stabilised ferrites and 3D printed composites, *Compos. Part B Eng.* 243 (2022). <https://doi.org/10.1016/j.compositesb.2022.110126>.
- [12] N. Ambikeswari, S. Manivannan, Superior magnetodielectric properties of room temperature synthesized superparamagnetic cobalt ferrite – graphene oxide composite, *J. Alloys Compd.* 763 (2018) 711–718. <https://doi.org/10.1016/j.jallcom.2018.05.275>.
- [13] T. Ram, A. Kumar, K. Khanna, S.K. Dwivedi, S. Kumar, Structural, magnetic, dielectric and magneto-dielectric response in $\text{Pb}_{0.75}\text{La}_{0.25}\text{TiO}_3\text{-CoFe}_2\text{O}_4$ composites, *Mater. Today Proc.* (2023).
- [14] M. Kurian, S. Thankachan, Structural diversity and applications of spinel ferrite core - Shell nanostructures- A review, *Open Ceram.* 8 (2021). <https://doi.org/10.1016/j.oceram.2021.100179>.
- [15] P.A. Vinosha, A. Manikandan, A.S. Judith, A. Dinesh, G.F. Nirmala, A.C. Preetha, Y. Slimani, M.A. Almessiere, A. Baykal, B. Xavier, Review on recent advances of zinc substituted cobalt ferrite nanoparticles : Synthesis characterization and diverse applications, *Ceram. Int.* 47 (2021) 10512–10535.
- [16] T. Kavinkumar, D. Sastikumar, S. Manivannan, Effect of functional groups on dielectric, optical gas sensing properties of graphene oxide and reduced graphene oxide at room temperature, *RSC Adv.* 5 (2015) 10816–10825. <https://doi.org/10.1039/c4ra12766h>.
- [17] M.N. Akhtar, M. Yousaf, Y. Lu, M.Z. Mahmoud, J. Iqbal, M.A. Khan, M.U. Khallidooon, S. Ullah, M. Hussien, Magnetic, structural, optical band alignment and conductive analysis of graphene-based REs (Yb, Gd, and Sm) doped NiFe_2O_4 nanocomposites for emerging technological applications, *Synth. Met.* 284 (2022) 1–9. <https://doi.org/10.1016/j.synthmet.2021.116994>.
- [18] X. Zhou, Y. Zhou, L. Zhou, J. Wei, J. Wu, D. Yao, Effect of Gd and La doping on the structure, optical and magnetic properties of NiZnCo ferrites, *Ceram. Int.* 45 (2019) 6236–6242. <https://doi.org/10.1016/j.ceramint.2018.12.102>.

- [19] T. Zhu, S. Chang, Y.F. Song, M. Lahoubi, W. Wang, PVP-encapsulated CoFe₂O₄/rGO composites with controllable electromagnetic wave absorption performance, *Chem. Eng. J.* 373 (2019) 755–766. <https://doi.org/10.1016/j.cej.2019.05.079>.
- [20] I. Childres, L.A. Jauregui, W. Park, H. Caoa, Y.P. Chena, Raman spectroscopy of graphene and related materials, *New Dev. Phot. Mater. Res.* (2013) 403–418.
- [21] A. Ur, N.A. Morley, N. Amin, M. Imran, M. Ajaz, K. Mahmood, A. Ali, A. Aslam, A. Bibi, M. Zahir, F. Iqbal, N. Bano, M. Alzaid, Controllable synthesis of La³⁺ doped Zn_{0.5}Co_{0.25}Cu_{0.25}Fe_{2-x}La_xO₄ (x = 0.0, 0.0125, 0.025, 0.0375, 0.05) nano-ferrites by sol-gel auto-combustion route, *Ceram. Int.* 4 (2020) 0–1. <https://doi.org/10.1016/j.ceramint.2020.08.106>.
- [22] H. Chouaya, M. Smari, I. Walha, E. Dhahri, M.P.F. Graça, M.A. Valente, The effect of bismuth on the structure, magnetic and electric properties of Co₂MnO₄ spinel multiferroic, *J. Magn. Magn. Mater.* 451 (2018) 344–350. <https://doi.org/10.1016/j.jmmm.2017.11.068>.
- [23] G. Abbas, A.U. Rehman, W. Gull, M. Afzaal, N. Amin, L. Ben Farhat, M. Amami, N.A. Morley, M. Akhtar, M.I. Arshad, A. Ghuffar, A. Mahmood, M. Ibrahim, Impact of Co²⁺ on the spectral, optoelectrical, and dielectric properties of Mg_{0.25}Ni_{0.25}Cu_{0.5-x}CoxFe_{1.97}La_{0.03}O₄ ferrites prepared via sol-gel auto-combustion route, *J. Sol-Gel Sci. Technol.* 101 (2022) 428–442. <https://doi.org/10.1007/s10971-021-05713-9>.
- [24] M.N. Akhtar, K. Ali, A. Umer, T. Ahmad, M.A. Khan, Structural elucidation, and morphological and magnetic behavior evaluations, of low-temperature sintered, Ce-doped, nanostructured garnet ferrites, *Mater. Res. Bull.* 101 (2018) 48–55. <https://doi.org/10.1016/j.materresbull.2018.01.009>.
- [25] S. Iranshahi, S. Mosivand, Cobalt/graphene oxide nanocomposites: Electro-synthesis, structural, magnetic, and electrical properties, *Ceram. Int.* 48 (2022) 12240–12254. <https://doi.org/10.1016/j.ceramint.2022.01.086>.
- [26] M. Farooq, A. Latif, S. Ajmal, M. Shahid, A. Sattar, M. Azhar, M. Asghar, M.F. Aly, Mg_{0.8}Ca_{0.2}NdxFe_{2-x}O₄-graphene nano-heterostructures for various potential applications, *Synth. Met.* 232 (2017) 8–16.
- [27] W. Shen, B. Ren, S. Wu, W. Wang, X. Zhou, Facile synthesis of rGO/SmFe₅O₁₂/CoFe₂O₄ ternary nanocomposites: Composition control for superior broadband microwave absorption performance, *Appl. Surf. Sci.* 453 (2018) 464–476.

<https://doi.org/10.1016/j.apsusc.2018.05.150>.

- [28] E.H. El-Khawas, A.A. Azab, A.M. Mansour, Structural, magnetic and dielectric properties of reduced graphene oxide/ $\text{La}_{0.9}\text{Bi}_{0.1}\text{FeO}_3$ nanocomposites, *Mater. Chem. Phys.* 241 (2020) 122335. <https://doi.org/10.1016/j.matchemphys.2019.122335>.
- [29] F.H. Mohammadabadi, S.M. Masoudpanah, S. Alamolhoda, H.R. Koohdar, Structure, magnetic, and microwave absorption properties of $(\text{MnNiCu})_{0.9-x}\text{Co}_x\text{Zn}_{0.1}\text{Fe}_2\text{O}_4$ /graphene composite powders F., *J. Alloys Compd.* 404–406 (2021) 1. <https://doi.org/10.1016/j.jallcom.2005.05.002>.
- [30] Y. Wang, L. Yao, Q. Zheng, M.-S. Cao, Graphene-wrapped multiloculated nickel ferrite: a highly efficient electromagnetic attenuation material for microwave absorbing and green shielding, *Nano Res.* 15 (2022) 6751–6760.
- [31] R. Shu, J. Xu, Z. Wan, X. Cao, Synthesis of hierarchical porous nitrogen-doped reduced graphene oxide/zinc ferrite composite foams as ultrathin and broadband microwave absorbers, *J. Colloid Interface Sci.* 608 (2022) 2994–3003. <https://doi.org/10.1016/j.jcis.2021.11.030>.
- [32] K. Qian, Z. Yao, H. Lin, J. Zhou, A. Ali, T. Qi, W. Chen, X. Guo, The influence of Nd substitution in Ni – Zn ferrites for the improved microwave absorption properties, *Ceram. Int.* 46 (2020) 227–235.
- [33] A. Aslam, A.U. Rehman, N. Amin, M. Ajaz un Nabi, Q. ul ain Abdullah, N.A. Morley, M.I. Arshad, H.T. Ali, M. Yusuf, Z. Latif, K. Mehmood, Lanthanum doped $\text{Zn}_{0.5}\text{Co}_{0.5}\text{La}_x\text{Fe}_{2-x}\text{O}_4$ spinel ferrites synthesized via co-precipitation route to evaluate structural, vibrational, electrical, optical, dielectric, and thermoelectric properties, *J. Phys. Chem. Solids.* 154 (2021) 110080. <https://doi.org/10.1016/j.jpcs.2021.110080>.
- [34] R. Shu, J. Zhang, C. Guo, Y. Wu, Z. Wan, J. Shi, Y. Liu, M. Zheng, Facile synthesis of nitrogen-doped reduced graphene oxide/nickel-zinc ferrite composites as high-performance microwave absorbers in the X-band, *Chem. Eng. J.* 384 (2020) 123266. <https://doi.org/10.1016/j.cej.2019.123266>.
- [35] J. Gao, Z. Ma, F. Liu, X. Weng, K. Meng, Preparation and microwave absorption properties of Gd–Co ferrite@silica@carbon multilayer core–shell structure composites, *Chem. Eng. J.* 446 (2022). <https://doi.org/10.1016/j.cej.2022.137157>.
- [36] F. Hosseini Mohammadabadi, S.M. Masoudpanah, S. Alamolhoda, H.R. Koohdar,

- Electromagnetic microwave absorption properties of high entropy spinel ferrite ((MnNiCuZn) $_{1-x}$ CoxFe $_2$ O $_4$)/graphene nanocomposites, *J. Mater. Res. Technol.* 14 (2021) 1099–1111. <https://doi.org/10.1016/j.jmrt.2021.07.018>.
- [37] A. Goldman, MODERN FERRITE TECHNOLOGY, 2006. https://doi.org/10.1007/978-0-387-29413-1_16.
- [38] M.M. Hossen, S. Nasrin, M.B. Hossen, *Physica B : Physics of Condensed Matter* Effect of Mn $^{2+}$ doping on structural , magnetic and electrical properties of combustion method for high-frequency applications, *Phys. B Phys. Condens. Matter.* 599 (2020) 412456.
- [39] K. Mehmood, A.U. Rehman, N. Amin, N.A. Morley, M.I. Arshad, Graphene nanoplatelets/Ni-Co-Nd spinel ferrite composites with improving dielectric properties, *J. Alloys Compd.* 930 (2023). <https://doi.org/10.1016/j.jallcom.2005.05.002>.
- [40] R. Ali, M.H. Aziz, S. Gao, M.I. Khan, F. Li, T. Batool, F. Shaheen, B. Qiu, Graphene oxide/zinc ferrite nanocomposite loaded with doxorubicin as a potential theranostic medium in cancer therapy and magnetic resonance imaging, *Ceram. Int.* 48 (2022) 10741–10750. <https://doi.org/10.1016/j.ceramint.2021.12.290>.
- [41] M.K. Kokare, N.A. Jadhav, Y. Kumar, K.M. Jadhav, S.M. Rathod, Effect of Nd $^{3+}$ doping on structural and magnetic properties of Ni $_{0.5}$ Co $_{0.5}$ Fe $_2$ O $_4$ nanocrystalline ferrites synthesized by sol-gel auto combustion method, *J. Alloys Compd.* 748 (2018) 1053–1061. <https://doi.org/10.1016/j.jallcom.2018.03.168>.
- [42] S.A. Habib, S.A. Saafan, T.M. Meaz, M.A. Darwish, D. Zhou, M.U. Khandaker, M.A. Islam, H. Mohafez, A. V. Trukhanov, S. V. Trukhanov, M.K. Omar, Structural, Magnetic, and AC Measurements of Nanoferrites/Graphene Composites, *Nanomaterials.* 12 (2022) 1–19. <https://doi.org/10.3390/nano12060931>.
- [43] A. Riaz, M. Azhar, M. Junaid, S. Gulbadan, A. Manzoor, S. Rabia, G. Abbas, H.H. Somaily, M. Morsi, T. Alshahrani, Effect of Nd $^{3+}$ ions on structural , spectral , magnetic , and dielectric properties of Co – Zn soft ferrites synthesized via sol-gel technique, *Mater. Chem. Phys.* 290 (2022).
- [44] M.A. Almessiere, Y. Slimani, M. Sertkol, F.A. Khan, M. Nawaz, H. Tombuloglu, E.A. Al-Suhaimi, A. Baykal, Ce–Nd Co-substituted nanospinel cobalt ferrites: An investigation of their structural, magnetic, optical, and apoptotic properties, *Ceram. Int.* 45 (2019) 16147–16156. <https://doi.org/10.1016/j.ceramint.2019.05.133>.

- [45] M.N. Akhtar, M.S. Nazir, M.A. Khan, S. Ullah, M.A. Assiri, Preparations and characterizations of Ca doped Ni–Mg–Mn nanocrystalline ferrites for switching field high-frequency applications, *Ceram. Int.* 48 (2022) 3833–3840. <https://doi.org/10.1016/j.ceramint.2021.10.167>.
- [46] S. Rahman, K. Nadeem, M. Anis-Ur-Rehman, M. Mumtaz, S. Naeem, I. Letofsky-Papst, Structural and magnetic properties of ZnMg-ferrite nanoparticles prepared using the co-precipitation method, *Ceram. Int.* 39 (2013) 5235–5239. <https://doi.org/10.1016/j.ceramint.2012.12.023>.